Chinese Chemical Letters 35 (2024) 109809

Contents lists available at ScienceDirect

Chinese Chemical Letters

journal homepage: www.elsevier.com/locate/cclet

Constructing multifunctional deep-blue emitters with weak charge transfer excited state for high-performance non-doped blue OLEDs and single-emissive-layer hybrid white OLEDs

Hui Liu[a,b,1], Xiangyang Tang[a,1], Zhuang Cheng[a], Yin Hu[a], Yan Yan[a], Yangze Xu[a], Zihan Su[a], Futong Liu[a,*], Ping Lu[a,*]

[a] State Key Laboratory of Supramolecular Structure and Materials Department of Chemistry, Jilin University, Changchun 130012, China
[b] Sichuan Province Key Laboratory of Information Materials and Devices Application, College of Optoelectronic Engineering, Chengdu University of Information Technology, Chengdu 610225, China

ARTICLE INFO

Article history:
Received 31 December 2023
Revised 16 March 2024
Accepted 20 March 2024
Available online 29 March 2024

Keywords:
Deep-blue emitters
Phenanthro[9,10]imidazole
Hot exciton
Host
Single-emissive-layer white device

ABSTRACT

Deep-blue emitter with high photoluminescence efficiency (PLQY) is highly desirable in ultra-high definition displays and white solid-state lightings. In this work, two deep-blue phenanthro[9,10]imidazole derivatives, PPIS and PPPIS, with hot exciton property are successfully developed. Compared to PPIS, the embedded phenyl bridge in PPPIS is able to effectively increase the overlap of frontier molecular orbitals. In consequence, PPPIS shows higher oscillator strength and significantly enhanced PLQY. PPPIS also achieves better electroluminescence performance in non-doped device, showing deep-blue emission with Commission International de l'Eclairage (CIE) coordinates of (0.153, 0.087) and the maximum external quantum efficiency (EQE_{max}) of 8.5% with minuscule efficiency roll-off. Meanwhile, when PPPIS serves as the host for phosphor PO-01, high-efficiency orange phosphorescent device is obtained with high EQE_{max} of 29.8% and negligible efficiency roll-off at 1000 cd/m^2. Further, efficient single-emissive-layer white device is assembled *via* utilizing PPPIS as a blue emitter as well as the host for PO-01 simultaneously, providing warm-white emission with CIE coordinates of (0.429, 0.433) at 1000 cd/m^2, the forward-viewing EQE_{max} of 27.2% and maximum power efficiency (PE_{max}) of 80.1 lm/W, respectively. Our studies can establish a viable design strategy for deep-blue emitters in high-performance non-doped blue OLEDs and hybrid WOLEDs.

Organic light-emitting diodes (OLEDs) possess considerable merits, such as wide color gamut, self-luminescence, quick response, transparency, flexibility, and have been applied in ultra-high definition (UHD) displays and solid-state lightings in recent years [1–4]. However, there still exist some bottlenecks hampering their further wide-scale commercialization. One crucial factor is the scarcity of high-performance deep-blue emitters, which not merely provide one of the three primary colors, but also can serve as the host for generating green, red and white emissions through energy transfer to emissive dopants [5–7]. In addition, deep-blue dyestuff plays a key role in reducing power consumption, achieving high color gamut and resolution in display and lighting applications [8–12]. Although the noble-metal-containing phosphorescent emitters could harvest all triplet excitons, it is hard to acquire impressive device performance in deep-blue region due to the heightened nonradiative process by metal d-orbitals [13–16]. Besides, blue phosphors often encounter stability problem due to weak chemical coordination bonds [17,18]. Except for phosphor materials, thermally activated delayed fluorescent (TADF) materials also can make use of all excitons *via* the reverse intersystem crossing (RISC) process from the lowest triplet (T_1) state to the lowest singlet (S_1) state [19–23]. However, because of the strong charge transfer (CT) character of S_1 state, their spectra generally show large stokes shift and big full widths at half maximum (FWHM), damaging color purity of blue emission [24,25]. In 2016, multi-resonance (MR) TADF materials with planar and rigid molecular structure are proposed to overcome the broad emission of typical donor-acceptor (D-A) type TADF materials, which has been the recent concern in OLEDs [26]. A series of MR-TADF materials that can cover the full-color visible range have been developed rapidly [27–31]. However, deep-blue MR-TADF emitters still remain very limited. In addition, most phosphorescent materials and MR-TADF

* Corresponding authors.
E-mail addresses: liuft@jlu.edu.cn (F. Liu), lup@jlu.edu.cn (P. Lu).
[1] These authors contributed equally to this work.

https://doi.org/10.1016/j.cclet.2024.109809
1001-8417/

materials have to be doped into proper host with wide energy-gap, which usually leads to complicated device configuration, complex fabrication procedure and severe efficiency roll-off [32,33]. Therefore, it is important to develop deep-blue fluorescent emitters with high-efficiency and suitability for non-doped devices.

Besides the utilization of triplet excitons from T_1 state *via* RISC process, transferring triplet excitons from high-lying triplet (T_n) state is another promising pathway to realize full exciton utilization, which has already been achieved in hot exciton emitters with hybridized local and charge transfer (HLCT) excited state character [34,35]. Benefiting from fast high-lying RISC (hRISC) process, these materials theoretically could realize high EQEs at high current density in non-doped devices. More importantly, when the S_1 state mainly manifests as the locally excited (LE) state rather than a CT state, hot exciton materials are likely to realize high-efficiency emission in deep-blue zone [36,37].

Phenanthroimidazole (PI) is a specific functional group for the construction of blue hot exciton materials owing to the large energy level splitting between T_1 and T_n [38]. Ma and co-workers reported an efficient hot exciton emitter PAC based on the skeleton of PI-anthracene (An), achieving a maximum external quantum efficiency (EQE_{max}) exceeding 10% with pure-blue emission in non-doped device [39]. Later, they modulated the electroluminescence (EL) spectrum to deep-blue region with an EQE_{max} of 6.76% by changing the linkage fashion between the PI and An core [40]. Recently, our group developed two deep-blue emitters, PIAnTPh and PyIAnTPh, through introduction of terphenyl unit to the skeleton described above, which showed high EQE_{max} over 8%, low Commission International de l'Eclairage (CIE) *y* value below 0.8, as well as narrow FWHM of about 50 nm [41]. However, these An-containing emitters all possess relatively low T_1, which restricts their application as the host materials. By contrast, deep-blue PI derivatives with high efficiency and moderate T_1 energy level may show versatility both as emitter and phosphor host, which provides wider application value, especially in the single-emissive-layer white devices [42,43]. Considering that PI group possesses ambipolar property and near-ultraviolet emission with decent photoluminescence (PL) efficiency, efficient deep-blue materials with high T_1 value are possible to be achieved *via* introducing neutral groups to regulate the molecular conjugation and excited state properties. Herein, two hot exciton materials with deep-blue emission, PPIS and PPPIS, are designed and synthesized by attaching a neutral diphenyl sulfide block to the horizontal backbone of PI unit. Both of them show fine PLQYs, high T_1 values, and LE-dominated HLCT excited state characters. As compared with PPIS, the inserted phenyl bridge entitles PPPIS with more CT component, higher oscillator strength and enhanced PL efficiency. As a result, PPPIS exhibits deep-blue emission with CIE coordinates of (0.153, 0.087) and superior EL efficiency with EQE_{max} of 8.5% in non-doped device. In addition, the orange phosphorescent OLED employing PPPIS as the host for PO-01 shows excellent EQE_{max} of 29.8% and a tiny efficiency roll-off of only 4.4% at 1000 cd/m^2. Furthermore, high-performance warm-white OLEDs are successfully achieved by doping PO-01 into PPPIS at low concentration in a single emitting layer, providing excellent maximum forward-viewing EQE of 27.2% and power efficiency (PE) value of 80.1 lm/W, respectively. These phosphorescent and white OLEDs are among the best devices results with the similar colors reported in the literatures (Tables S2 and S3 in Supporting information).

The synthesis pathways of PPIS and PPPIS are illustrated in Scheme S1 (Supporting information). The key precursor PPIB was attained in high yield according to previous reports [37]. PPIS and PPPIS were obtained by "one-pot" reaction and Suzuki coupling reaction, respectively. The purity and chemical structure of final products were fully verified by NMR, mass spectrum and elemental analysis. As shown in Fig. S5 (Supporting information) and

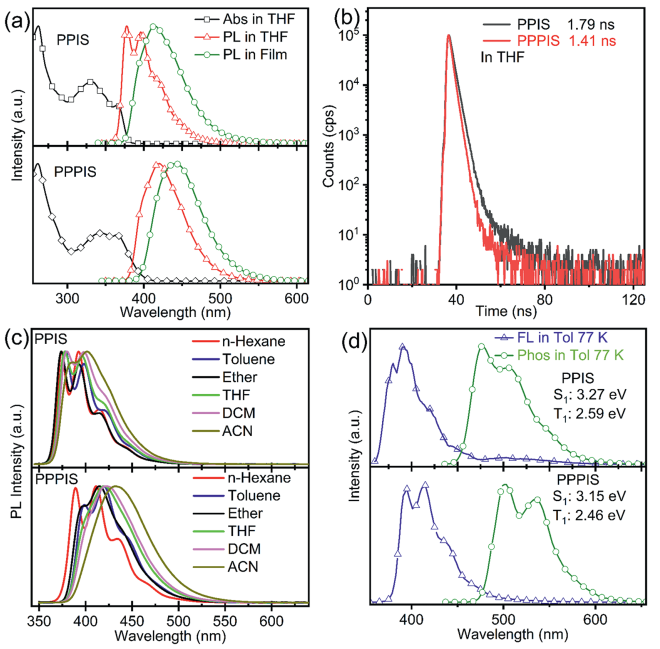

Fig. 1. (a) UV–vis absorption and PL spectra of PPIS and PPPIS in dilute THF solution and neat films. (b) Luminescence decay curves of PPIS and PPPIS in dilute THF solution. (c) Solvatochromic PL spectrums of PPIS and PPPIS. (d) Fluorescence and phosphorescence spectra of PPIS and PPPIS in toluene at 77 K.

Table 1, PPIS and PPPIS possessed high decomposition temperature (T_d) of 417 °C and 427 °C, respectively. The melting point temperatures (T_m) of PPIS and PPPIS were 209 °C and 223 °C, respectively. Thermal analyses demonstrated that incorporation of benzene bridge in PPPIS contributed to the notable enhancements in both thermal and morphological stabilities. The electrochemical properties of PPIS and PPPIS were evaluated using cyclic voltammetry (CV) measurements. According to the Eqs. S1 and S2 (Supporting information), the onset for oxidation and reduction potentials with respect to the ferrocenium/ferrocene (Fc^+/Fc) redox couple were utilized to determine the highest occupied molecular orbital (HOMO) and lowest unoccupied molecular orbital (LUMO) energy levels, which were calculated to be −5.51 eV and −2.21 eV for PPIS, and −5.50 eV and −2.38 eV for PPPIS, respectively. These results suggest that the insertion of benzene bridge could lower the LUMO energy level, thereby facilitating electron injection in device, which is beneficial for balanced charge recombination and promising device performance [44].

To investigate their photophysical properties, the absorption and PL spectra of PPIS and PPPIS in dilute tetrahydrofuran (THF) solution and non-doped film were measured. As shown in Fig. 1a, the broad absorption bands between 300 nm and 400 nm were assigned to the π–π^* transitions from the conjugated molecular backbone [36]. Because of the enlarged π-conjugation, the absorption spectrum of PPPIS became slightly broader and bathochromic-shifted than PPIS, implying a higher CT component in the system. As expected, PPIS and PPPIS both showed deep-blue emission in THF and thin films. The PL spectrum of PPPIS displayed the maximum emission peak at 410 nm in THF, slightly red-shifted compared to PPIS (370 nm) owing to the extended π-conjugation. As shown in Fig. 1b, both PPIS and PPPIS showed the single-exponential fluorescence decays in THF with lifetimes in nanosecond scale, ruling out the possibility of TADF process. The PLQY of PPPIS in THF reached 98.1%, which was much higher than that of PPIS (61.4%). demonstrating that the inserted phenyl bridge could significantly improve the PLQY. Besides, the absolute PLQYs of PPIS and PPPIS in various solvents were very high, indicating the HLCT

Table 1
Key physical properties of PPIS and PPPIS.

Emitter	T_d/T_g (°C)	$\lambda_{abs,max}$ (nm) [a]	λ_{PL} (nm) [b]		S_1/T_1 [c] (eV)	HOMO/LUMO (eV) [d]	PLQY (%) [e]	
			sol	film			sol	film
PPIS	417/209	365	378, 394, 419	412	3.27/2.59	−5.51/−2.21	61.4	40.5
PPPIS	427/223	366	420	442	3.15/2.46	−5.50/−2.38	98.1	75.3

[a] The first absorption peak in dilute THF solution (10^{-5} mol/L) at room temperature.
[b] Fluorescent emission peak in THF and thin film.
[c] Estimated from the first peak of the fluorescence and phosphorescence spectra in toluene at 77 K.
[d] Estimated by cyclic voltammetry measurement.
[e] Evaluated using an integrating sphere.

state was a highly emissive excited state which was beneficial for promising device performance. It is noteworthy that the PL spectrum of PPIS in THF exhibited clear fine vibrational structure, which became much vague in the spectrum of PPPIS, illustrating that these two molecules possessed different excited state properties.

To further concretely compare the excited state properties of PPIS and PPPIS, solvatochromic PL spectra were measured. As displayed in Fig. 1c, with an increase in solvent polarity, the PL spectra of PPIS revealed well-resolved fine vibronic structure in all solvents and the emission peaks performed a slight red-shift of approximately 10 nm, indicating the primary character of S_1 state in PPIS is predominantly a LE state, accompanied by a minor contribution of CT component. For PPPIS, the PL spectra only exhibited well-resolved fine vibrational structure in low-polarity solvents, while the fine vibronic structure almost disappeared in acetonitrile (ACN) and the red-shift of emissive peak from n-hexane to ACN enhanced to 21 nm, proving that more CT component existed in S_1 state of PPPIS. The obtained results aligned with the typical features observed in LE-dominated HLCT excited states and proved that the strategy of regulating excited states through the insertion of benzene ring is feasible [45]. Lippert-Mataga plots were performed to investigate the HLCT properties of the chromophores by the function of the Stokes shifts with the orientation polarizability of solvents (Fig. S8 in Supporting information). Two-section linear relations were both observed for PPIS and PPPIS in low- and high-polarity solvents, indicating the co-existence of two different excited state characters as well as the formation of HLCT states in PPIS and PPPIS. The Lippert-Mataga plots also supported the occurrence of non-equivalent hybridization between different excited states.

To evaluate the potential of PPIS and PPPIS as hosts in application of phosphor and simplified white devices, fluorescence and phosphorescence spectra in toluene were measured at 77 K (Fig. 1d). The S_1 and T_1 values of PPIS were determined to be 3.27 and 2.59 eV, respectively, which were both higher than that of PPPIS (3.15 and 2.46 eV). Such large energy gap between S_1 and T_1 for PPIS and PPPIS (0.68 and 0.69 eV) also could exclude the probability of TADF process. Although the insertion of a phenyl conjugation slightly lowered the T_1 value of PPPIS, the T_1 of 2.46 eV was still obviously higher the that of phosphor PO-01 (2.2 eV), which could guarantee the positive-going energy transfer from fluorescent host to phosphor guest and the application of PPPIS as host in phosphor and hybrid-white devices [42].

To determine their excited state differences at the theoretical level, the natural transition orbitals of singlet and triplet states were calculated and analyzed using time-dependent density functional theory with the B3lyp/6–31G(d,p) method. As depicted in Fig. 2, for PPIS, the hole was localized on the PPI moiety and sulfur atom, and the distribution of particle was almost identical to the hole with an elongation to the N-position connected benzene ring, which was a typical LE-dominated HLCT state [45]. By contrast, for PPPIS, although the hole and particle were both delocal-

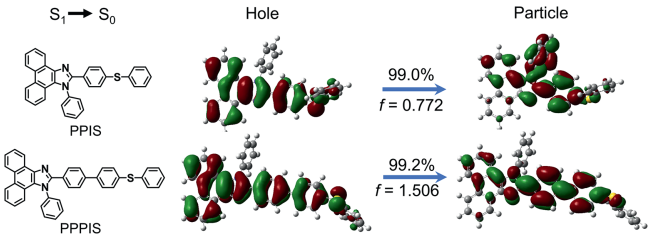

Fig. 2. The natural transition orbitals and properties of $S_1 \rightarrow S_0$ for PPIS and PPPIS.

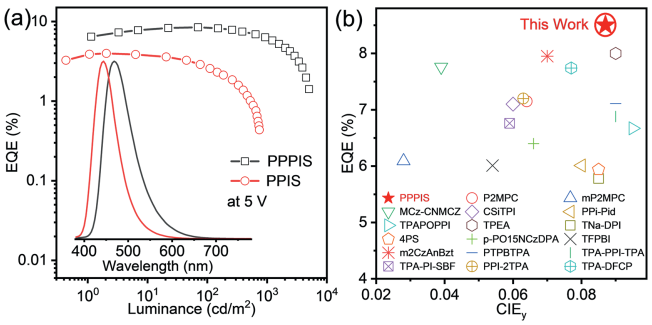

Fig. 3. (a) EQEs *vs.* luminance curve, inset: EL spectra at 5 V. (b) Plots of EQE_{max} against CIE_y coordinate of the representative deep-blue non-doped fluorescent OLEDs. The details of these devices and their references are listed in Table S1 (Supporting information).

ized on the whole molecule except for terminal phenyl ring, more orbital separation could be observed in the phenanthrene as well as biphenyl unit, suggesting that PPPIS also had an LE-dominated HLCT transition character but with a higher CT proportion than PPIS in S_1 state. These results aligned with the phenomenon observed in the solvatochromic PL spectra. Moreover, it is worth noting that PPPIS demonstrated larger oscillator strengths of 1.506 than PPIS (0.772) owing to the extended hole-electron overlap on the inserted phenyl ring, which was in accordance with the measured higher PLQY in PPPIS.

To get insight into the potential of PPIS and PPPIS as blue emitters, non-doped OLEDs were fabricated. The device energy level diagrams were presented in Fig. S12 (Supporting information) and the key device data were summarized in Table 2. As shown in Fig. 3, the devices of PPIS and PPPIS (corresponding to device B1 and B2) both showed deep-blue emission peaking at 436 nm and 444 nm with the corresponding CIE coordinates of (0.158, 0.061) and (0.153, 0.087), respectively, which approached the National Television Standards Committee blue standard CIE coordinates of (0.14, 0.08). The turn-on voltage (V_{on}) of device B1 and B2 were 3.4 V and 2.9 V, respectively. The lower V_{on} and higher current density of device B2 should be attributed to the embedded phenyl ring conjugation in PPPIS, which reduced LUMO energy level. Furthermore, device B2 showed higher maximum EQE of 8.5% and the EQE at the luminance of 1000 cd/m^2 could still reach 6.3%, displaying a

Table 2
Key OLEDs performance parameters.

Emitter	V_{on} (V) [a]	L_{max} (cd/m^2) [b]	CE (cd/A) [c]	PE (lm/W) [c]	EQE (%) [c]	EL λ_{max} (nm) [d]	CIE (x,y) [e]
B1	3.4	744	2.3	2.0	4.0/-	436	0.158, 0.061
B2	2.9	5037	6.6/4.6	6.3/2.6	8.5/6.3	444	0.153, 0.087
O	2.7	124,849	88.3/84.1	90.8/69.0	29.8/28.5	564	0.504, 0.491
W	2.8	30,357	78.5/63.0	80.1/50.8	27.2/22.3	–	0.429, 0.433

[a] Turn-on voltage at a luminance of 1 cd/m^2.
[b] Maximum luminance.
[c] Maximum efficiencies and values taken at 1000 cd/m^2.
[d] EL λ_{max}: EL emission peak of EL spectrum at 1000 cd/m^2.
[e] CIE: Commission International de l'Eclairage coordinates at 1000 cd/m^2.

low device efficiency roll-off. Only by the insertion of a single conjugated phenyl ring, PPPIS showed significantly enhanced device performance than PPIS. Considering that the PLQYs of PPIS and PPPIS (40.5% and 75.3%) in thin film, their exciton utilization efficiencies in devices obviously exceeded upper-limit (25%) of traditional fluorescent emitters, thus there must exist utilization channel of triplet excitons. Firstly, the TADF process could be easily excluded on the basis of the large energy gap between S_1 and T_1 (~0.69 eV) and nanosecond decay of PPIS and PPPIS (Figs. 1b and d). In addition, the linear relations between the EL luminance and the current density (Fig. S15 in Supporting information) demonstrated that the triplet–triplet annihilation (TTA) process was not dominant at low current density and the triplet exciton transformation from TTA mechanism was negligible. Therefore, high exciton utilization efficiency should be derived from the hRISC process of hot exciton materials. Based on the energy levels of the excited state (Fig. S9 in Supporting information), both PPIS and PPPIS exhibited a significant T_2/T_3-T_1 energy level gap, along with small energy splitting between S_1 and T_2/T_3, which all presented HLCT characteristics. The large spin-orbit coupling (SOC) values between T_2/T_3 and S_1 states of PPPIS were 0.67 and 0.50 cm^{-1}, which could effectively enhance the hRISC process, while the SOC matrix element values between T_2/T_3 and S_1 states were just 0.61 and 0.13 cm^{-1} for PPIS. PPPIS had a more effective hRISC channel causing by the stronger SOC, thus, the non-doped device achieved higher performance. Besides, the insertion of benzene ring in PPPIS effectively enhanced the PLQY and reduced the LUMO level, which gave rise to a lowered electron injection barrier and better energy level matching between the emissive layer and electron transporting layer. The electron mobilities of PPPIS and PPIS were determined under the same condition to be 1.166×10^{-5} and 2.908×10^{-5} cm^2 V^{-1} s^{-1}, while the hole mobilities were 3.904×10^{-5} and 8.483×10^{-6} cm^2 V^{-1} s^{-1}, respectively. The bipolar carrier-transporting ability of PPPIS was beneficial to enhance the carrier recombination efficiency and broaden the recombination zone. All these factors resulted in the higher efficiency in PPPIS-based blue OLED.

In above sections, PPPIS showed superior blue OLED performance and balanced carrier transport ability (Fig. S16 in Supporting information). To further exploit its potential as the host of phosphorescent dyes, PPPIS was employed as the host for the orange phosphor PO-01. As shown in Fig. S17 (Supporting information), the PL spectrum of PPPIS exhibited large spectral overlap with the absorption of PO-01, indicating the efficient energy transfer from host to guest could occur. In addition, the T_1 of PPPIS reached 2.46 eV, which was higher than that of PO-01 and thus could guarantee the energy transfer from host to the PO-01 and avoid energy loss. The phosphorescent device O demonstrated yellow-orange emission peaking at 564 nm and excellent device efficiency with maximum LE, EQE and PE of 88.3 cd/A, 29.8% and 90.8 lm/W, respectively. In addition, the EQE at 1000 cd/m^2 was still as high as 28.5%, showing the negligible efficiency roll-off. These superior device performances confirmed that PPPIS is a suitable host for the phosphorescence dopant.

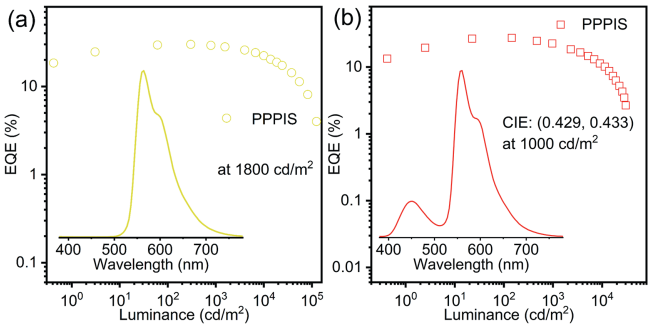

Fig. 4. (a) EQE *vs.* luminance curve of orange phosphorescent device; inset: EL spectra at 1800 cd/m^2. (b) EQE *vs.* luminance curve of hybrid WOLEDs; inset: EL spectra at 1000 cd/m^2.

We further explored its potential applications in hybrid white organic light-emitting diodes (WOLEDs) by doping PO-01 into PPPIS at a low concentration in the single-emissive-layer. Accordingly, the WOLEDs based on PPPIS were fabricated with the configuration of ITO/TAPC (30 nm)/TCTA (10 nm)/PPPIS: 0.8 wt% PO-01 (20 nm)/TmPyPb (40 nm)/LiF (1 nm)/Al (100 nm). The white device performance was shown in Fig. 4 and Table 2. Device W exhibited a low V_{on} of 2.8 V and superior efficiencies with forward-viewing CE, EQE and PE up to 78.5 cd/A, 27.2% and 80.1 lm/W, respectively. In addition, the EQE still could keep high EQE of 22.3% at 1000 cd/m^2. This device showed warm-white emission with CIE coordinates of (0.429, 0.433) at 1000 cd/m^2, which is of high potential as a healthy lighting source. Device W showed a dominant orange emission peak and the blue emission peak changed with the luminance increased from 500 cd/m^2 to 13,000 cd/m^2, which might be related to the direct charge carrier trapping on the phosphorescent guest PO-01. The shallower HOMO and deeper LUMO of PO-01, compared to PPPIS, enabled it to preferentially capture the hole and electron, which facilitated the direct formation of excitons on the guest molecule. Additionally, trap-assisted recombination likely occurred on PO-01 molecules due to their narrower bandgap compared to the PPPIS molecule, leading to the orange emission [46,47].

In summary, we reported two deep-blue emitters, PPIS and PPPIS, with fine PLQYs, high T_1 energy levels, and LE-dominated HLCT excited state characters. Benefiting from the embedded phenyl ring conjugation, PPPIS demonstrates more CT ingredient, higher oscillator strength and enhanced PL efficiency than PPIS. Meanwhile, superior EL performance with EQE_{max} of 8.5% is also achieved in non-doped device of PPPIS, accompanied by deep-blue emission with CIE coordinates of (0.153, 0.087). In addition, by constructing an emitting layer system, PPPIS dopped by PO-01, high-efficiency orange phosphorescent device and single-emitting-layer WOLED are obtained, achieving the superior EQE of 29.8% and 27.2%, respectively. Those excellent EL performances of PPPIS in deep-blue, phosphorescent, and white OLEDs not only manifest the outstand-

ing potential in display and lighting devices, but also provides a simple but effective avenue for developing highly efficient deep-blue emitters applicable in non-doped blue and simplified white devices.

Declaration of competing interest

The authors declare that they have no known competing financial interests or personal relationships that could have appeared to influence the work reported in this paper.

CRediT authorship contribution statement

Hui Liu: Data curation, Writing – original draft. **Xiangyang Tang:** Conceptualization. **Zhuang Cheng:** Formal analysis. **Yin Hu:** Validation. **Yan Yan:** Investigation. **Yangze Xu:** Methodology. **Zihan Su:** Validation. **Futong Liu:** Funding acquisition, Writing – review & editing. **Ping Lu:** Funding acquisition, Writing – review & editing.

Acknowledgments

The authors acknowledge financial support from National Natural Science Foundation of China (No. 22075100), the Jilin Provincial Science and Technology Department (No. 20220201082GX), the China Postdoctoral Science Foundation (Nos. 2022TQ0111, 2023M731267), Sichuan Science and Technology Program (No. 2023NSFSC0985), Scientific Research Foundation of Chengdu University of Information Technology (No. KYTZ202174) and the Changsha Automobile Innovation Research Institute.

Supplementary materials

Supplementary material associated with this article can be found, in the online version, at doi:10.1016/j.cclet.2024.109809.

References

[1] H.W. Chen, J.H. Lee, B.Y. Lin, et al., Light: Sci. Appl. 7 (2018) 17168.
[2] J. Song, H. Lee, E.G. Jeong, et al., Adv. Mater. 32 (2020) 1907539.
[3] G. Hong, X. Gan, C. Leonhardt, et al., Adv. Mater. 33 (2021) 2005630.
[4] Y. Huang, E.L. Hsiang, M.Y. Deng, et al., Light: Sci. Appl. 9 (2020) 105.
[5] D. Chen, W. Li, L. Gan, et al., Mater. Sci. Eng. R 142 (2020) 100581.
[6] J.H. Lee, C.H. Chen, P.H. Lee, et al., J. Mater. Chem. C 7 (2019) 5874–5888.
[7] Y. Im, S.Y. Byun, J.H. Kim, et al., Adv. Funct. Mater. 27 (2017) 1603007.
[8] X. Chen, J.W. Zhao, X. H, et al., Chin. Chem. Lett. 30 (2019) 1989–1993.
[9] B. Li, X.a. Song, X. Jiang, et al., Chin. Chem. Lett. 31 (2020) 1188–1192.
[10] Z. Wu, D. Ma, Mater. Sci. Eng. R 107 (2016) 1–42.
[11] V. Jankus, C.J. Chiang, F. Dias, et al., Adv. Mater. 25 (2013) 1455–1459.
[12] D.H. Ahn, S.W. Kim, H. Lee, et al., Nat. Photonics 13 (2019) 540–546.
[13] J. Lee, M. Slootsky, K. Lee, et al., Light: Sci. Appl. 3 (2014) e181.
[14] D. Ma, T. Tsuboi, Y. Qiu, et al., Adv. Mater. 29 (2016) 1603253.
[15] C. Wu, Y. Zhang, J. Miao, et al., Chin. Chem. Lett. 34 (2023) 107445.
[16] J.S. Huh, M.J. Sung, S.K. Kwon, et al., Adv. Funct. Mater. 31 (2021) 2100967.
[17] J. Jayabharathi, V. Thanikachalam, S. Thilagavathy, Coord. Chem. Rev. 483 (2023) 215100.
[18] C.F.R. Mackenzie, L. Zhang, D.B. Cordes, et al., Adv. Opt. Mater. 11 (2023) 2201495.
[19] J. Chen, J. Zeng, X. Zhu, et al., CCS Chem. 3 (2021) 230–240.
[20] J.U. Kim, I.S. Park, C.Y. Chan, et al., Nat. Commun. 11 (2020) 1765.
[21] X. Tang, L.S. Cui, H.C. Li, et al., Nat. Mater. 19 (2020) 1332–1338.
[22] H. Uoyama, K. Goushi, K. Shizu, et al., Nature 492 (2012) 234–238.
[23] U. Balijapalli, R. Nagata, N. Yamada, et al., Angew. Chem. Int. Ed. 60 (2021) 8477–8482.
[24] X. Hu, Y. Qin, Z. Li, et al., Chin. Chem. Lett. 33 (2022) 4645–4648.
[25] J. Liu, Z. Feng, C. Peng, et al., Chin. Chem. Lett. 34 (2023) 107634.
[26] T. Hatakeyama, K. Shiren, K. Nakajima, et al., Adv. Mater. 28 (2016) 2777–2781.
[27] X.C. Fan, K. Wang, Y.Z. Shi, et al., Nat. Photonics 17 (2023) 280–285.
[28] Y. Kondo, K. Yoshiura, S. Kitera, et al., Nat. Photonics 13 (2019) 678–682.
[29] Y. Zou, J. Hu, M. Yu, et al., Adv. Mater. 34 (2022) 2201442.
[30] M. Yang, I.S. Park, T. Yasuda, J. Am. Chem. Soc. 142 (2020) 19468–19472.
[31] F. Liu, Z. Cheng, Y. Jiang, et al., Angew. Chem. Int. Ed. 61 (2022) e202116927.
[32] F. Liu, Z. Cheng, L. Wan, et al., Small 18 (2021) 2106462.
[33] Y. Zhang, D. Zhang, J. Wei, et al., Angew. Chem. Int. Ed. 58 (2019) 16912–16917.
[34] W. Li, D. Liu, F. Shen, et al., Adv. Funct. Mater. 22 (2012) 2797–2803.
[35] Y. Xu, P. Xu, D. Hu, et al., Chem. Soc. Rev. 50 (2021) 1030–1069.
[36] C. Du, T. Lu, Z. Cheng, et al., J. Mater. Chem. C 10 (2022) 14186–14193.
[37] C. Du, H. Liu, Z. Cheng, et al., Adv. Funct. Mater. 33 (2023) 2304854.
[38] J. Tagare, S. Vaidyanathan, J. Mater. Chem. C 6 (2018) 10138–10173.
[39] Y. Xu, X. Liang, X. Zhou, et al., Adv. Mater. 31 (2019) 1807388.
[40] Y. Xu, X. Liang, Y. Liang, et al., ACS Appl. Mater. Interfaces 11 (2019) 31139–31146.
[41] F. Liu, Z. Cheng, L. Wan, et al., Chem. Eng. J. 426 (2021) 131351.
[42] C. Cao, W.C. Chen, J.X. Chen, et al., ACS Appl. Mater. Interfaces 11 (2019) 11691–11698.
[43] C. Liu, T. Li, M. Sun, et al., Adv. Funct. Mater. 33 (2023) 2215066.
[44] X. Tang, Q. Bai, T. Shan, et al., Adv. Funct. Mater. 28 (2018) 1705813.
[45] H. Zhang, A. Li, G. Li, et al., Adv. Opt. Mater. 8 (2020) 1902195.
[46] D. Zhang, M. Cai, Y. Zhang, et al., ACS Appl. Mater. Interfaces 7 (2015) 28693–28700.
[47] Z. Xu, Y. Gong, Y. Dai, et al., Adv. Opt. Mater. 7 (2019) 1801539.